Special Feature: Materials Analysis Using Quantum Beams

Research Report

Measurement of Energy Bands at Semiconductor Surfaces and Interfaces by Hard X-ray Photoelectron Spectroscopy

Keita Kataoka, Tetsuo Narita, Daigo Kikuta and Shin Tajima

Report received on May 13, 2015

ABSTRACT Energy bands at semiconductor surfaces and interfaces are important for characterizing various electronic properties. We demonstrated measurement techniques for the valence band offset (VBO) and band bending using hard X-ray photoelectron spectroscopy (HAXPES). Because the photoelectron escape depth for HAXPES is larger than that for conventional X-ray photoelectron spectroscopy, the energy band can be measured nondestructively using thicker real-device-like samples. The VBO of the CdS/CZTS interface was successfully estimated by a new analysis method using only valence band spectra. The band bending for *p*-type GaN was analyzed before and after inductively coupled plasma etching, using takeoff-angle-dependent photoelectron spectra. The present techniques can be applied to various branches of semiconductor materials research.

KEYWORDS HAXPES, Photoelectron Spectroscopy, Band Offset, Band Bending, Semiconductor Interface, Semiconductor Surface, CZTS, GaN, Inductively Coupled Plasma Etching

1. Introduction

Many semiconductor devices owe their functions to specific electronic properties at interfaces.[1] For instance, metal-insulator-semiconductor (MIS) transistors can function as an electronic switch through the formation of a depleted layer or inversion layer at the insulator/semiconductor interface by gate insulator-mediated bias control. The rectifying function for carriers (Schottky barrier diode and *p-n* diode) and the photovoltaic function (solar cells) result from the discontinuity of the energy bands and the potential gradient. Because the energy bands at the interface determine the device properties, the band position and shape are important.

Energy bands are often sensitively modulated by surface- or interface-specific effects. The reconstructed surface structure,[2] interface reactive layer,[3] interface altered-layer,[4] and adhesion of contaminations[5] can be induced by film formation, annealing, dry etching, wet treatment, or ion implantation. Thus, energy band measurement is an effective way to investigate the influence of different processes on device properties.

The valence band offset (VBO) can be determined experimentally by X-ray photoelectron spectroscopy (XPS).[6] This method has been widely applied to a variety of heterojunction interfaces[7-9] using a conventional XPS system with Al $K\alpha$ ($h\upsilon$ = 1486.6 eV) or Mg $K\alpha$ ($h\upsilon$ = 1253.6 eV) X-ray sources. Under these experimental conditions, the inelastic mean free path (IMFP) λ,[10] i.e., the effective photoelectron escape depth, is restricted to approximately 2-4 nm owing to strong inelastic scattering of photoelectrons. As a result, a heterojunction sample with an extremely thin top layer having a thickness close to the IMFP is needed.[6-9] The problem is that the VBO for a thin heterojunction sample does not always correspond to that for a real device. Therefore, it is preferable to measure the VBO using a sample with a top layer having a thickness close to that of a real device.

A large photoelectron escape depth is needed for thicker heterojunction samples. By raising the X-ray photon energy for excitation, the escape depth can be extended. In recent years, hard X-ray photoelectron spectroscopy (HAXPES) was developed using a synchrotron light source with a high photon flux.[11] HAXPES achieves a larger escape depth due to the higher kinetic energy of photoelectrons. For instance, the IMFP for Si 1*s* photoelectrons in SiO_2 is extended to approximately 13 nm for $h\upsilon$ = 8 keV.[10] In the case of conventional XPS with Al $K\alpha$, the IMFP for Si 2*p* photoelectrons in SiO_2 is approximately

© Toyota Central R&D Labs., Inc. 2015

3.8 nm. The VBO values for more real-device-like thicker heterojunction samples can be measured nondestructively by HAXPES.

Furthermore, the larger escape depth makes it possible to investigate energy band bending in near-surface or near-interface regions. In most previous studies using conventional XPS,[12-14] only the surface Fermi level position was measured because of the small escape depth. In HAXPES, the energy band position can be obtained over an extended escape depth by measuring the takeoff angle dependence.

In this study, we demonstrate the suitability of HAXPES for VBO and band bending measurements. For VBO measurement, an interface was prepared between CdS and Cu_2ZnSnS_4 (CZTS).[15] CZTS thin films are promising for use in high-efficiency, low-cost, nontoxic and rare-metal-free photovoltaic solar cells.[16-18] A CdS/CZTS layered structure is often used to obtain a higher open circuit voltage and to separate rapidly generated electron-hole pairs. The conduction band offset (CBO) for the CdS/CZTS interface is important because it determines the electron transport properties.

For band bending measurements, Mg-doped *p*-type GaN was prepared.[19] Inductively coupled plasma (ICP) etching is commonly used for GaN-based power devices. However, it is well known that etching damage is introduced into GaN.[20-22] It is necessary to determine the effects of ICP etching on the GaN surface in order to suppress or undo the etching-induced damage. We measured the changes in band bending of the *p*-type GaN surface before and after ICP etching.

2. Techniques for Measurement of the Energy Band by HAXPES

2. 1 Determination of the Valence Band Offset

In principle, the energy positions of photoelectron spectra are determined relative to the Fermi level, which is defined as 0 eV in binding energy. The onset of the valence band (VB) spectrum corresponds to the valence band maximum (VBM) in reference to the Fermi level. Because the Fermi levels for the two materials at the heterojunction interface are spontaneously adjusted by charge exchange to coincide with each other, the VBO corresponds to the difference in the VBM of the two materials.

It is difficult to resolve the two different onsets from a mixed VB spectrum for the heterojunction sample. In general, the onsets for materials A and B can be experimentally determined as follows.[6] **Figure 1** shows schematic band diagrams for materials A and B, and for the heterojunction interface. The VB onsets ($E_{VBM}{}^{A}$ and $E_{VBM}{}^{B}$) and the core level peaks ($E_{CL}{}^{A}$ and $E_{CL}{}^{B}$) are measured independently. The energy differences ($E_{CL\text{-}VBM}{}^{A} = E_{CL}{}^{A} - E_{VBM}{}^{A}$) and ($E_{CL\text{-}VBM}{}^{B} = E_{CL}{}^{B} - E_{VBM}{}^{B}$) are specific to materials A and B, respectively. Therefore, using the core level peaks obtained for the heterojunction sample ($E_{CL}{}^{A(A+B)}$ and $E_{CL}{}^{B(A+B)}$), the VBM ($E_{VBM}{}^{A(A+B)}$ and $E_{VBM}{}^{B(A+B)}$) are given by

$$E_{VBM}{}^{A(A+B)} = E_{CL}{}^{A(A+B)} - E_{CL\text{-}VBM}{}^{A} \quad (1)$$

$$E_{VBM}{}^{B(A+B)} = E_{CL}{}^{B(A+B)} - E_{CL\text{-}VBM}{}^{B}, \quad (2)$$

and VBO is given by

$$\begin{aligned} E_{VBO} &= E_{VBM}{}^{A(A+B)} - E_{VBM}{}^{B(A+B)} \\ &= (E_{CL}{}^{A(A+B)} - E_{CL\text{-}VBM}{}^{A}) - (E_{CL}{}^{B(A+B)} - E_{CL\text{-}VBM}{}^{B}). \quad (3) \end{aligned}$$

In addition to the general method described above, we developed a new method to determine the VBO.[15] As shown in **Fig. 2**, the VB spectra for materials A and B ($VB_A(E)$ and $VB_B(E)$) are measured independently. The heterojunction sample provides a mixed VB spectrum ($VB_{A+B}(E)$) for materials A and B. By fitting using a linear combination of $VB_A(E)$ and $VB_B(E)$, the difference in the VB onsets for materials A and B yields the VBO. The objective function for the fit can be expressed as follows:

$$VB_{A+B}(E) = a \times VB_A(E + c) + b \times VB_B(E + d), \quad (4)$$

where a, b, c, and d are constants (fitting parameters). This is more a direct method because VBO is determined using only the VB spectra.

2. 2 Analysis Method for Band Bending

Figure 3 shows a schematic band diagram with upward band bending toward a surface or interface. The core levels have the same energy shift as the VB or conduction band (CB). Therefore, the shift in the energy band position is reflected in the shift in the core level peak. The band bending shape can be estimated on the basis of takeoff-angle-dependent core level

© Toyota Central R&D Labs., Inc. 2015

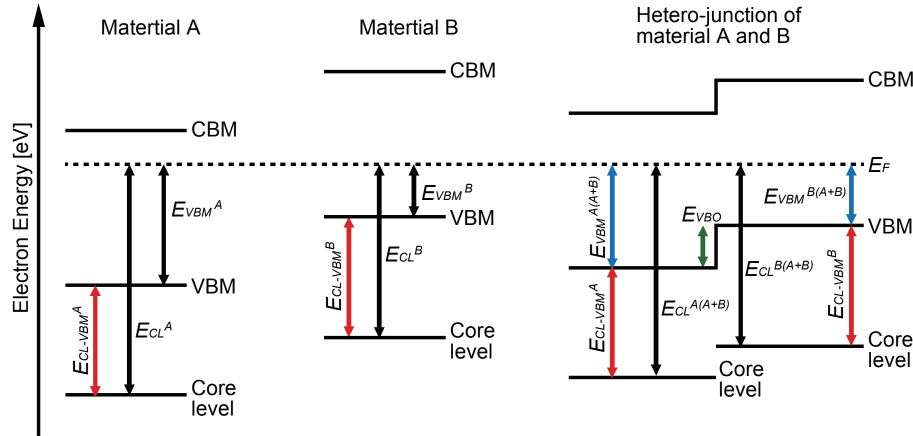

Fig. 1 Schematic energy band diagram obtained through measurement of the valence band offset by photoelectron spectroscopy. Since the energy difference between E_{CL} and E_{VBM} is constant, the valence band offset of the heterojunction sample can be obtained experimentally.

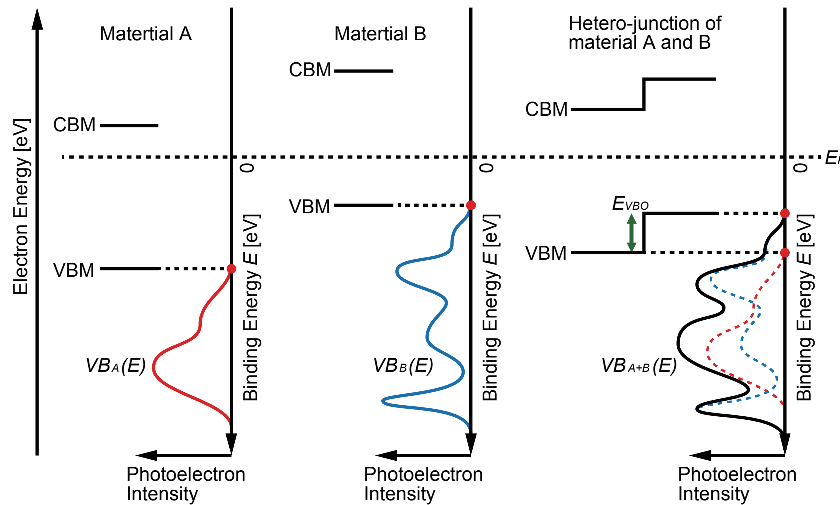

Fig. 2 Schematic energy band diagram and valence band (VB) spectra obtained through the measurement of the valence band offset by photoelectron spectroscopy. The mixed VB spectrum ($VB_{A+B}(E)$) consists of the sum of $VB_A(E)$ and $VB_B(E)$.

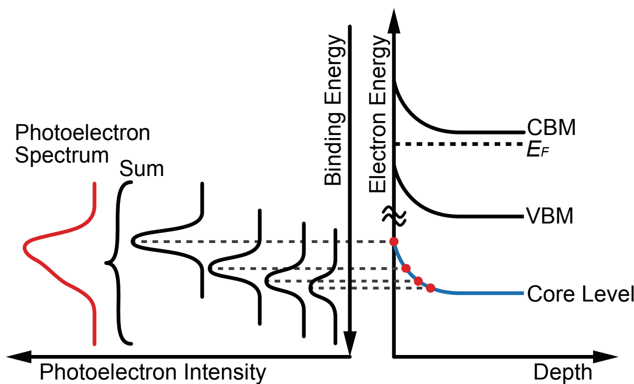

Fig. 3 Schematic energy band diagram with upward band bending toward the surface and the corresponding photoelectron spectrum of the core level.

spectra as follows. The effective analysis depth (λ_{eff}), i.e., the component of IMFP[10] perpendicular to the surface, is:

$$\lambda_{eff} = \lambda \sin \theta, \tag{5}$$

where θ is the takeoff angle measured from the surface. The photoelectron intensity (I_{PE}) emitted at a depth x decreases exponentially with x as:

$$I_{PE}(x) = I_0 \exp(-x/\lambda_{eff}), \tag{6}$$

where I_0 is the photoelectron intensity at $x = 0$. The core level spectrum can be interpreted as the integrated

© Toyota Central R&D Labs., Inc. 2015

spectrum emitted from a given depth. Each spectrum can be approximated by a Gaussian function. Thus, the core level spectrum $F(E, x)$ can be expressed as

$$F(E, x) = \int_0^\infty \left[I_{PE}(x) \times exp\left(- \frac{(E - E_{bending}(x))^2}{2\sigma^2} \right) \right] dx, \quad (7)$$

where E is the photoelectron energy and $E_{bending}(x)$ is a function of the band bending shape. The band bending shape can be quantitatively analyzed by applying Eq. (7) to the takeoff-angle-dependent spectra.

3. Experimental Details and Sample Preparation

HAXPES measurements were carried out at the BL46XU and BL47XU beam lines of Spring-8. The excitation X-ray photon energy was approximately 8 keV. We observed the photoelectron spectra of Cu $2p_{3/2}$ and the VB region for CZTS, the photoelectron spectra of Cd $3d_{5/2}$ and the VB region for CdS, and the photoelectron spectra of Ga $2p_{3/2}$ and N $1s$ for GaN. The λ values calculated by TPP-2M[10] were about 17, 12, 9.0, and 9.7 nm for Cu $2p_{3/2}$ in CZTS, Cd $3d_{5/2}$ in CdS, Ga $2p_{3/2}$ in GaN, and N $1s$ in GaN, respectively. The takeoff angles of photoelectrons were 80° for CZTS and CdS, and 80°, 40°, and 12° for GaN. All photoelectron spectra were calibrated using an Au film deposited on a Si substrate. The Fermi edge for Au was defined as 0.00 eV in binding energy.

For the VBO measurement of the CdS/CZTS interface, CdS (5 nm)/CZTS (700 nm)/Mo/glass, CZTS (700 nm)/Mo/glass, and CdS (100 nm)/CZTS (700 nm)/Mo/glass were prepared. The buried CZTS layer of CdS (5 nm)/CZTS (700 nm) was measurable, thanks to the larger IMFP. CZTS (700 nm) and CdS (100 nm)/CZTS (700 nm) were used as standards for CZTS and CdS, respectively. The roughly 700-nm-thick CZTS layers were formed by sulfurizing a CZTS precursor using H_2S gas. CdS buffer layers were deposited on the CZTS layers by chemical bath deposition and subsequently annealed at 473 K under a N_2 atmosphere. The details of CZTS cell fabrication have been reported elsewhere.[18]

In the band bending measurements for GaN, unetched and ICP-etched Mg-doped *p*-type GaN samples were prepared using conventional metalorganic chemical vapor deposition on *a*-plane sapphire substrates. A 2-μm-thick *p*-type GaN film doped with 2.5×10^{19} cm^{-3} Mg was grown on a 1-μm-thick unintentionally-doped GaN buffer layer. An activation anneal was performed at 850°C. The ICP etching gas mixture was Cl_2 and BCl_3, used at a flow rate of 25 and 5 cm^3/min, respectively, under 1 Pa pressure. ICP etching was performed at an antenna power of 300 W and a bias power of 30 W.

4. Results and Discussion

4. 1 The Valence Band Offset for the CdS/CZTS Interface

First, we estimated the VBO using the conventional method. We measured the core levels and VB spectra for the CZTS and CdS standards. The energy difference between the Cu $2p_{3/2}$ peak (E_{CL}^{CZTS}) and the VB onset (E_{VB}^{CZTS}) for the CZTS sample ($E_{CL}^{CZTS} - E_{VB}^{CZTS}$) was 931.67 eV. The energy difference between the Cd $3d_{5/2}$ peak (E_{CL}^{CdS}) and the VB onset (E_{VB}^{CdS}) for the CdS sample ($E_{CL}^{CdS} - E_{CL}^{CdS}$) was 403.35 eV. The VB onsets were determined by linear extrapolation of the leading edges of the VB spectra. For CdS (5 nm)/CZTS (700 nm), the Cu $2p_{3/2}$ peak for the CZTS layer and the Cd $3d_{5/2}$ peak for the CdS layer were measured; the results are shown in **Fig. 4**. The Cu $2p_{3/2}$ peak ($E_{CL}^{CZTS(CZTS+CdS)}$) and the Cd $3d_{5/2}$ peak ($E_{CL}^{CdS(CZTS+CdS)}$) were 932.14 and 404.94 eV, respectively. By using Eqs. (1) to (3), the VBO was estimated to be 1.1 ± 0.1 eV.

Next, the new method was employed to estimate the VBO by using Eq. (4). **Figure 5** shows the curve fit obtained for the VB spectrum of CdS (5 nm)/CZTS (700 nm), using the VB spectra of the CZTS and CdS standards. The fit was in excellent agreement with the VB spectrum of the heterojunction sample. Thus, the VBO was estimated to be 1.0 ± 0.1 eV, which agrees within experimental error with the VBO obtained by using the core level peaks. This indicates that the new method is useful for VBO estimation.

In photoelectron spectroscopy, it often happens that charging due to X-ray irradiation becomes a problem because it induces a shift in the energy band. The charging effect can be monitored by measuring the photoelectron peak shift as a function of the X-ray photon flux. In our case, energy shifts on the order of several tens of meV were found for all samples. However, for CdS (5 nm)/CZTS (700 nm), the magnitude of the peak shifts for the Cu $2p_{3/2}$ and Cd $3d_{5/2}$ levels were the same at the same X-ray photon flux. This indicates that the VBO was not changed by

© Toyota Central R&D Labs., Inc. 2015

charging, although the absolute energy position with reference to the Fermi level could not be obtained.

Figure 6 shows the experimentally obtained schematic energy band diagram for the CdS/CZTS interface. The band gap was estimated to be 2.4 and 1.4 eV for CdS and CZTS, by using optical absorption and external quantum efficiency measurements, respectively. Using the band gaps, a CBO of 0.0 ± 0.1 eV was obtained. This was slightly different from previously reported values.(23-25) It has been reported that the surface condition of the CZTS layer has no influence on the CBO.(25) Therefore, the CBO presumably depends on the film formation conditions or the quality of the CdS layer.

4. 2 Band Bending for ICP-etched *p*-type GaN

Figure 7 shows takeoff-angle dependent Ga $2p_{3/2}$ and N 1*s* spectra of unetched and ICP-etched *p*-type GaN. The spectra of both samples changed dramatically with takeoff angle. The N 1*s* spectra exhibited similar shapes to the Ga $2p_{3/2}$ spectra. Thus, the spectrum shapes reflect the shifts in the energy band due to the depth, rather than to the chemical bonding state. In the case of Ga $2p_{3/2}$ photoelectrons, the λ_{eff} values calculated by Eq. (5) are 8.8, 5.8, and 1.9 nm for takeoff angles of 80°, 40°, and 12°, respectively. For both samples, the Ga $2p_{3/2}$ level gradually shifted to a higher binding energy with decreasing λ_{eff}, which shows downward band bending toward the surface.

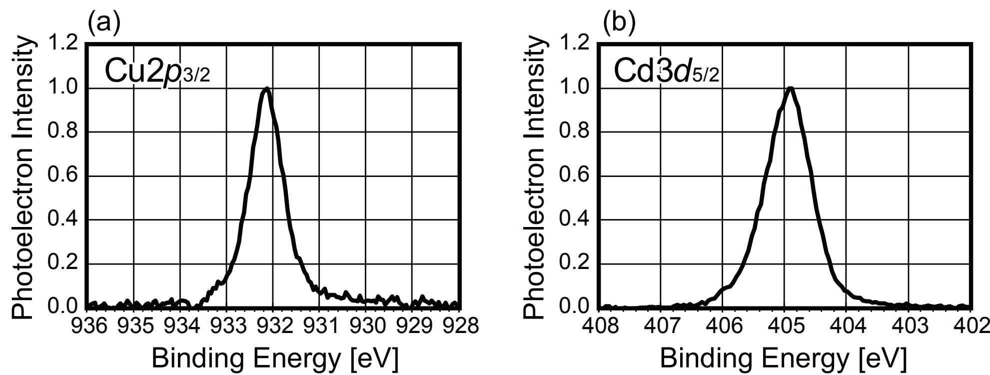

Fig. 4 HAXPES spectra of (a) Cu $2p_{3/2}$ and (b) Cd $3d_{5/2}$ levels obtained from the CdS (5 nm)/CZTS (700 nm) sample.

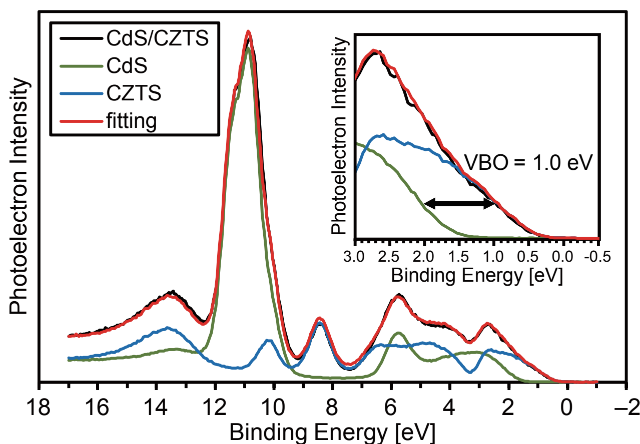

Fig. 5 Curve fit of the valence band (VB) spectrum for the heterojunction sample with CdS (5 nm)/CZTS (700 nm), using the VB spectra of the CZTS and CdS standards. Inset shows a blowup of the onset of the VB spectra.

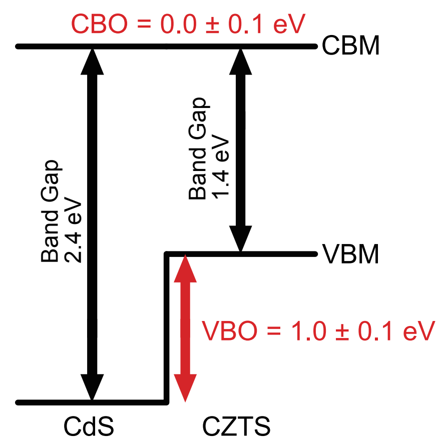

Fig. 6 Schematic energy band diagram of the CdS/CZTS interface, obtained by HAXPES.

© Toyota Central R&D Labs., Inc. 2015

We analyzed the band bending using Eq. (7). In our calculations, quadric band bending was assumed for $E_{bending}(x)$. The calculated spectra for the unetched sample well fitted the experimental results as shown in **Fig. 8**(a), when an acceptor concentration of 4.3×10^{19} cm^{-3} and a band bending potential of 1.8 eV were assumed. The calculated N 1*s* spectra also well fitted the experimental results using the same parameters. The acceptor concentration obtained was higher than the bulk Mg dopant concentration of 2.5×10^{19} cm^{-3}. The higher Mg concentration was consistent with the results of secondary ion mass spectroscopy. We believe that the higher Mg concentration in the near-surface region was due to Mg segregation. A band bending potential of 1.6 eV has been reported for a Mg concentration of 3×10^{19} cm^{-3}.[26] These values are comparable to our results.

For the ICP-etched sample, the spectra calculated by assuming quadric band bending were not consistent with the experimental results. Under the assumption of a surface layer with a deep donor concentration (see **Fig. 9**), rather than of quadric band bending, the calculated spectra well fitted the experimental results, as shown in Fig. 8(b). We believe that a high deep donor density above 1×10^{20} cm^{-3} is induced by ICP etching in the near surface region. The depth of the surface layer with a higher deep donor concentration was estimated to be approximately 8 nm.

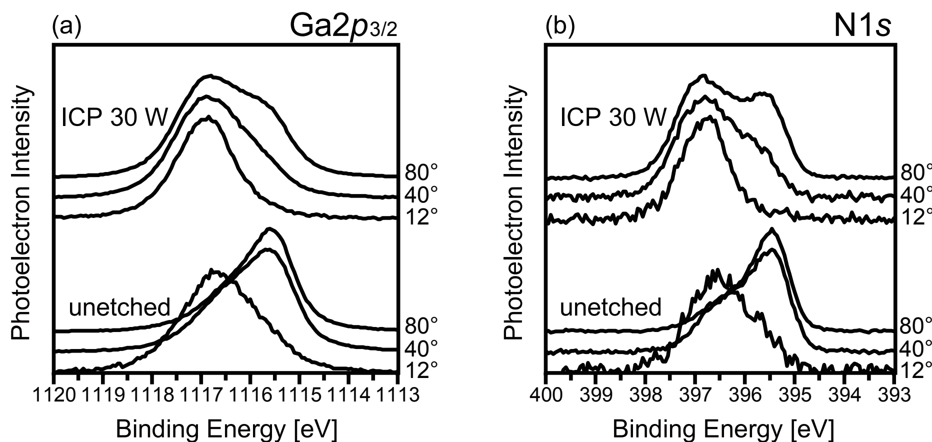

Fig. 7 HAXPES spectra of (a) the Ga 2$p_{3/2}$ and (b) N 1*s* levels as a function of the takeoff angle (TOA) of photoelectrons for unetched and ICP-etched *p*-type GaN. The spectra were measured at TOAs of 80°, 40°, and 12°. The *p*-type GaN films were etched by an inductively coupled plasma (ICP) with a bias power of 30 W.

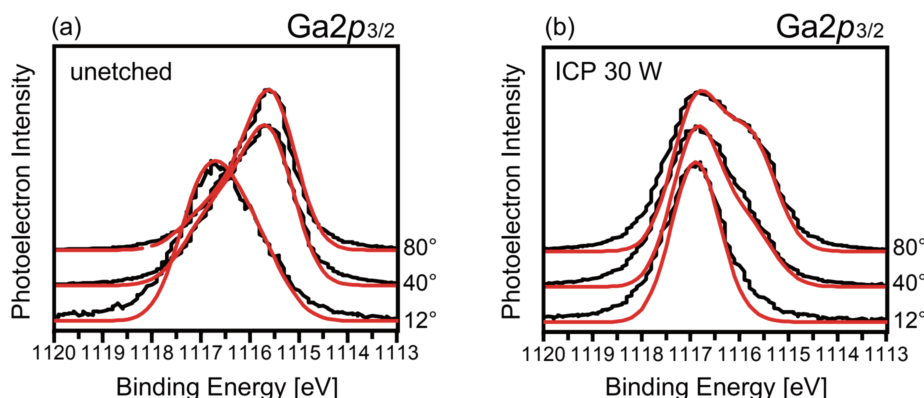

Fig. 8 The takeoff-angle-dependent HAXPES spectra (black solid lines) and calculated spectra (red solid lines) of the Ga 2$p_{3/2}$ level for (a) the unetched sample and (b) ICP-etched sample with a bias power of 30 W.

© Toyota Central R&D Labs., Inc. 2015

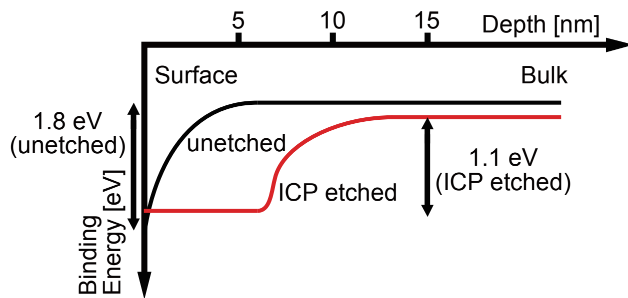

Fig. 9 Schematic band diagram obtained from the takeoff-angle-dependent HAXPES measurements for unetched and ICP-etched *p*-type GaN.

5. Summary

We have demonstrated VBO and band bending measurements at the CdS/CZTS interface and ICP-etched *p*-type GaN surface, respectively, by exploiting the deep photoelectron escape depth for HAXPES. A VBO of 1.0 ± 0.1 eV for the more real-device-like CdS/CZTS interface was successfully estimated by the new analysis method through curve fitting the VB spectra. A schematic band diagram was obtained for the CdS/CZTS interface by using VBO and band gaps. A detailed analysis of the shape of takeoff-angle-dependent core level spectra successfully yielded the band bending in the near-surface region of *p*-type GaN. This suggested the presence of a surface layer with higher deep donor concentration after ICP etching. The present results are expected to find wide applicability in energy band measurements of semiconductor interfaces and surfaces using HAXPES.

Acknowledgements

The experiments were performed at the BL47XU and BL46XU beam lines at Spring-8 with the approval of the Japan Synchrotron Radiation Research Institute (JASRI) (Proposal Nos. 2009B2008, 2010A1713, 2010A1805 and 2010B1781).

References

(1) Sze, S. M. and Ng, Kwok K., *Physics of Semiconductor Devices* (2007), 832p., John Willey & Sons, Inc., Hoboken, New Jersey.
(2) Takayanagi, K., Tanishiro, Y., Takahashi, S. and Takahashi, M., *Surf. Sci.*, Vol. 164, No. 2-3 (1985), pp. 367-392.
(3) Kataoka, K., Hattori, K., Miyatake, Y. and Daimon, H., *Phys. Rev. B*, Vol. 74, No. 15 (2006), 155406.
(4) Kataoka, K., Kimoto, Y., Horibuchi, K., Nonaka, T., Takahashi, N., Narita, T., Kanechika, M. and Dohmae, K., *Surf. Interface Anal.*, Vol. 44, No. 6 (2012), pp. 709-712.
(5) Ishikawa, H., Kobayashi, S., Koide, Y., Yamasaki, S., Nagai, S., Umezaki, J., Koike, M. and Murakami, M., *J. Appl. Phys.*, Vol. 81, No. 3 (1997), pp. 1315-1322.
(6) Kraut, E. A., Grant, R. W., Waldrop, J. R. and Kowalczyk, S. P., *Phys. Rev. Lett.*, Vol. 44, No. 24 (1980), pp. 1620-1623.
(7) Waldrop, J. R., Kraut, E. A., Farley, C. W. and Grant, R. W., *J. Appl. Phys.*, Vol. 69, No. 1 (1991), pp. 372-378.
(8) Cook, T. E., Fulton, C. C., Mecouch, W. J., Tracy, K. M., Davis, R. F., Hurt, E. H., Lucovsky, G. and Nemanich, R. J., *J. Appl. Phys.*, Vol. 93, No. 7 (2003), pp. 3995-4004.
(9) Edge, L. F., Schlom, D. G., Chambers, S. A., Cicerrella, E., Freeouf, J. L., Hollander, B. and Schubert, J., *Appl. Phys. Lett.*, Vol. 84, No. 5 (2004), pp. 726-728.
(10) Tanuma, S., Powell, C. J. and Penn, D. R., *Surf. Interface Anal.*, Vol. 21, No. 3 (1994), pp. 165-176.
(11) Kobayashi, K., Yabashi, M., Takata, Y., Tokushima, T., Shin, S., Tamasaku, K., Miwa, D., Ishikawa, T., Nohira, H., Hattori, T., Sugita, Y., Nakatsuka, O., Sakai, A. and Zaima, S., *Appl. Phys. Lett.*, Vol. 83, No. 5 (2003), pp. 1005-1007.
(12) Long, J. P. and Bermudez, V. M., *Phys. Rev. B*, Vol. 66, No. 12 (2002), 121308.
(13) Lau, W. M., Huang, L. J., Bello, I., Yiu, Y. M. and Lee, S. T., *J. Appl. Phys.*, Vol. 75, No. 7 (1994), pp. 3385-3391.
(14) Kim, J. K., Kim, K. J., Kim, B., Kim, J. N., Kwak, J. S., Park, Y. J. and Lee, J. L., *J. Electron. Mater.*, Vol. 30, No. 3 (2001), pp. 129-133.
(15) Tajima, S., Kataoka, K., Takahashi, N., Kimoto, Y., Fukano, T., Hasegawa, M. and Hazama, H., *Appl. Phys. Lett.*, Vol. 103, No. 24 (2013), 243906.
(16) Ito, K. and Nakazawa, T., *Jpn. J. Appl. Phys.*, Vol. 27, No. 11 (1988), pp. 2094-2097.
(17) Shin, B., Gunawan, O., Zhu, Y., Bojarczuk, N. A., Chey, S. J. and Guha, S., *Prog. Photovoltaics*, Vol. 21, No. 1 (2013), pp. 72-76.
(18) Fukano, T., Tajima, S. and Ito, T., *Appl. Phys. Express*, Vol. 6, No. 6 (2013), 062301.
(19) Narita, T., Kikuta, D., Takahashi, N., Kataoka, K., Kimoto, Y., Uesugi, T., Kachi, T. and Sugimoto, M., *Phys. Status Solidi A*, Vol. 208, No. 7 (2011), pp. 1541-1544.
(20) Kato, M., Mikamo, K., Ichimura, M., Kanechika, M., Ishiguro, O. and Kachi, T., *Jpn. J. Appl. Phys.*, Vol. 103, No. 9 (2008), 093701.
(21) Choi, K. J., Jang, H. W. and Lee, J. L., *Appl. Phys. Lett.*, Vol. 82, No. 8 (2003), pp. 1233-1235.

© Toyota Central R&D Labs., Inc. 2015

(22) Watanabe, H., Kato, M., Ichimura, M., Arai, E., Kanechika, M., Ishiguro, O. and Kachi, T., *Jpn. J. Appl. Phys*., Vol. 46, No. 1 (2007), pp. 35-39.
(23) Haight, R., Barkhouse, A., Gunawan, O., Shin, B., Copel, M., Hopstaken, M. and Mitzi, D. B., *Appl. Phys. Lett*., Vol. 98, No. 25 (2011), 253502.
(24) Nagoya, A., Asahi, R. and Kresse, G., *J. Phys. Cond. Matter*., Vol. 23, No. 40 (2011), 404203.
(25) Bär, M., Schubert, B.-A., Marsen, B., Wilks, R. G., Pookpanratana, S., Blum, M., Krause, S., Unold, T., Yang, W., Weinhardt, L., Heske, C. and Schock, H.-W., *Appl. Phys. Lett*., Vol. 99, No. 22 (2011), 222105.
(26) Hashizume, T., *J. Appl. Phys*., Vol. 94, No. 1 (2003), pp. 431-436.

Fig. 5
Reprinted from Applied Physics Letters, Vol. 103 (2013), 243906, Tajima, S., Kataoka, K., Takahashi, N., Kimoto, Y., Fukano, T., Hasegawa, M. and Hazama, H., © 2014 AIP, with permission from AIP Publishing LLC.

Keita Kataoka
Research Fields:
- Semiconductor Physics
- Surface and Interface Analysis
Academic Degree: Dr.Sci.

Tetsuo Narita
Research Field:
- III-Nitride Semiconductor: Growth, Power Device and Physics
Academic Degree: Dr.Sci.
Academic Society:
- The Japan Society of Applied Physics

Daigo Kikuta
Research Field:
- GaN-based Power Devices: Fabrication Process and Device Characterization
Academic Degree: Dr.Eng.
Academic Societies:
- The Japan Society of Applied Physics
- The Institute of Electronics, Information and Communication Engineers

Shin Tajima
Research Fields:
- Magnetic Materials
- Photovoltaic Materials
- Synthesis of Inorganic Materials
Academic Degree: Dr.Eng.
Academic Societies:
- The Ceramic Society of Japan
- The Japan Society of Applied Physics
- The Magnetics Society of Japan
- Japan Society of Powder and Powder Metallurgy
Awards:
- JSPM Distinguished Paper Award, 2005
- IEEE Photovoltaic Specialists Conference Best Poster Award, 2014

© Toyota Central R&D Labs., Inc. 2015